Nonparametric modeling of random uncertainties for dynamic response of mistuned bladed disks

Evangéline Capiez-Lernout, Christian Soize

Nonparametric modeling of random uncertainties for dynamic response of mistuned bladed-disks.

by

E. Capiez-Lernout [1] and **C. Soize** [2]

[1] Graduate student, Laboratory of Engineering Mechanics, University of Marne-La-Vallée, 5, Bd Descartes
77454 Marne-La-Vallée Cedex 02, France - E-mail: capiez@univ-mlv.fr

[2] Professor, Laboratory of Engineering Mechanics, University of Marne-La-Vallée, 5, Bd Descartes
77454 Marne-La-Vallée Cedex 02, France - E-mail: soize@univ-mlv.fr

Abstract

The random character of blade mistuning is a motivation to construct probability models of random uncertainties. Recently, a new approach known as a nonparametric model of random uncertainties, based on the entropy optimization principle, was introduced for modeling random uncertainties in linear and non-linear elastodynamics. This paper presents an extension of this nonparametric model for vibration analysis of structures with cyclic geometry. In particular this probability model allows the blade eigenfrequencies uncertainties and the blade-modal-shape uncertainties to be modeled.

1 Introduction

Structural dynamics of mistuned bladed-disks remain a difficult problem in turbomachinery. Usually, vibration analysis of cyclic structures is performed using their cyclic symmetry and is formulated for one sector from which the dynamics of the structure is reconstructed (see for instance [1, 2]). Nevertheless, manufacturing tolerances and dispersion of materials create uncertainties on geometry, boundary conditions and material properties of each blade. In the present paper, it is assumed that the disk is not mistuned. It is known that the phenomenon related to mistuning can induce strong vibrations for the forced response of the bladed-disk and can produce spatial localization in the dynamic response of the blades as proved in the early works [3, 4]. A good understanding of the mistuning effects still remains a subject of interest. Mistuning has been the object of various researches these last decades and many numerical studies have been developed on both free and forced responses. The influence of several parameters as interblade coupling, strength mistuning or damping has also been explored [5, 6, 7]. Moreover, the random nature of blade mistuning has been a motivation to construct probability models of random uncertainties to solve the corresponding stochastic responses and to perform statistical analyses in order to predict the effects of mistuning. Several researches have also been carried out to accurately estimate probability responses related to mistuning by using perturbation techniques with a simple lumped parameter models [8, 9]. Reduced order models have been extensively studied to reduce time costs for mistuned industrial turbomachinery bladed-disks [10, 11, 12]. In the context of the blade mistuning, a probabilistic parametric approach requires a complete probabilistic parametric description of the uncertain parameters, such as the use of stochastic fields for modeling uncertainties of constitutive equations, boundary conditions and

geometry. Such a probabilistic parametric method is not really simple to develop because of the large number of parameters which induce mistuning and which has to be identified. A good compromise widely used in most studies dealing with this subject, is to consider the Young modulus of blades as uncertain variables. In this case, blade eigenfrequencies are mistuned through the stiffness parameters but the corresponding eigenmodes remain unchanged with respect to the tuned case. Recently, Mignolet *et al.* [13, 14] introduced a probability model which is experimentally identified using the maximum likelihood principle in order to include blade-modal-shape mistuning or not. This model exhibits differences with respect to the parametric probability model currently used. Since the random character of blade mistuning is a motivation to construct probability models of random uncertainties, the present goal of this paper is to present an alternative nonparametric probability model to the usual parametric one for modeling random uncertainties in mistuning analysis. This nonparametric probabilistic approach allows both data uncertainties and model uncertainties to be taken into account while probabilistic parametric approaches do not allow model uncertainties to be modeled. Such a nonparametric approach has been recently introduced in linear elastodynamics, in time and frequency domain [15, 16]. This nonparametric probability model is directly constructed using the mean reduced matrix model, and using a probability model for symmetric positive-definite real random matrices, which is constructed using the entropy maximization principle with the available information. In section 2, the mean reduced matrix model required by the nonparametric approach is presented. Section 3 is devoted to the nonparametric model of random uncertainties. Section 4 describes the strategy for mistuning analysis. In section 5, a numerical example is given. In particular, a numerical comparison is carried out in order to give an information when the dispersion levels of the random matrices issued from the nonparametric and from the usual parametric approach are similar.

2 Construction of the mean reduced matrix model

Let Ω be a fixed structure with an N-order cyclic symmetry, submitted to external forces (the problem under consideration is related to rotating structures; in order to simplify the presentation, a fixed structure is considered; the methodology and the results presented can be extended without difficulty to the case of rotating structures). The geometrical domain, the viscoelasticity tensor, the mass density and the Dirichlet conditions related to the generating sector are invariant under the $2\pi/N$ rotation around the rotational axis of symmetry. Consequently, we are then interested in the linearized vibrations around a static equilibrium configuration considered as a natural state without prestresses whose model will be called the mean model of the structure. The vibration analysis is performed in the frequency band $\mathbb{B}$. Structure Ω is divided into one disk Ω_d and N identical blades Ω_j, for j belonging to $\{0, \ldots, N-1\}$. Let Σ_j be the coupling interface between blade Ω_j and disk Ω_d. It is assumed that the blades are only coupled by the disk. The disk is fixed on a part of its boundary. The mistuning is assumed to be statistically independent from blade to blade. Consequently, the nonparametric probability model of random uncertainties for a blade is described independently of the other blades. Furthermore, the probabilistic nonparametric approach requires the construction of a mean reduced matrix model for each uncertain substructure. This justifies the use of a dynamic substructuring method. The Craig & Bampton method [17] is used in this paper but any other substructuring methods could be used. Then, the mean finite element model of the disk is assembled with the mean reduced model of each blade. The resulting mean matrix model will be called the mean reduced matrix model for the bladed-disk. It should be outlined that the purpose of this paper is not to construct the most efficient reduced order model adapted to the mistuning problematic. This has been thoroughly studied in the literature. The focus of this paper deals with the model of mistuning by using a nonparametric probabilistic approach. Thus, the construction of this mean reduced model for each blade is only justified by the use of a nonparametric probability model for describing the blade random uncertainties. For ω fixed in frequency band $\mathbb{B}$, let $[\underline{A}^d(\omega)]$ be the mean dynamic stiffness matrix of disk Ω_d with free coupling interface. Let n_d be the number of DOFs of the disk. For the disk, the block decomposition with respect to the internal DOFs and with respect to the

coupling interface DOFs yields

$$[\underline{A}^d(\omega)] = \begin{bmatrix} [\underline{A}^d_{ii}(\omega)] & [\underline{A}^d_{i\Sigma}(\omega)] \\ [\underline{A}^d_{i\Sigma}(\omega)]^T & [\underline{A}^d_{\Sigma\Sigma}(\omega)] \end{bmatrix} \quad . \tag{1}$$

Each blade j is reduced by the Craig & Bampton decomposition method [17] with N_g fixed coupling interface modes. For ω fixed in frequency band $\mathbb{B}$, let $[\underline{A}^j_{\text{red}}(\omega)]$ be the mean reduced dynamic stiffness matrix of blade Ω_j with free coupling interface. Matrix $[\underline{A}^j_{\text{red}}(\omega)]$ is defined by

$$[\underline{A}^j_{\text{red}}(\omega)] = -\omega^2[\underline{M}^j_{\text{red}}] + i\omega[\underline{D}^j_{\text{red}}] + [\underline{K}^j_{\text{red}}] \quad , \tag{2}$$

and its block decomposition with respect to the N_g generalized coordinates $\underline{\mathbf{q}}^j$ and to the n_Σ coupling interface DOFs is written as

$$[\underline{A}^j_{\text{red}}(\omega)] = \begin{bmatrix} [\underline{A}^j(\omega)] & [\underline{A}^j_c(\omega)] \\ [\underline{A}^j_c(\omega)]^T & [\underline{A}^j_\Sigma(\omega)] \end{bmatrix} \quad . \tag{3}$$

Let $N_a = N_g + n_\Sigma$. The matrices $[\underline{M}^j_{\text{red}}] \in \mathbb{M}^+_{N_a}(\mathbb{R})$, $[\underline{D}^j_{\text{red}}] \in \mathbb{M}^{+0}_{N_a}(\mathbb{R})$ and $[\underline{K}^j_{\text{red}}] \in \mathbb{M}^{+0}_{N_a}(\mathbb{R})$ are the mean reduced mass, damping and stiffness matrices respectively. The mean vector of the physical DOFs is then given by

$$\begin{bmatrix} \underline{\mathbf{u}}^j_i(\omega) \\ \underline{\mathbf{u}}^j_\Sigma(\omega) \end{bmatrix} = [\underline{H}^j] \begin{bmatrix} \underline{\mathbf{q}}^j(\omega) \\ \underline{\mathbf{u}}^j_\Sigma(\omega) \end{bmatrix} \quad , \tag{4}$$

in which, for blade j, $[\underline{H}^j]$ is the transformation matrix involved by the Craig & Bampton decomposition [17], $\underline{\mathbf{u}}^j_i(\omega)$ is the mean vector of the internal DOFs and $\underline{\mathbf{u}}^j_\Sigma(\omega)$ is the mean vector of the coupling interface DOFs. The mean reduced matrix model of the bladed-disk is then obtained by assemblage which yields

$$\begin{bmatrix} [\underline{\mathcal{A}}(\omega)] & [\underline{A}_c(\omega)] & [\mathbb{0}] \\ [\underline{A}_c(\omega)]^T & [\underline{A}_\Sigma(\omega)] + [\underline{A}^d_{\Sigma\Sigma}(\omega)] & [\underline{A}^d_{i\Sigma}(\omega)]^T \\ [\mathbb{0}] & [\underline{A}^d_{i\Sigma}(\omega)] & [\underline{A}^d_{ii}(\omega)] \end{bmatrix} \begin{bmatrix} \underline{\mathbf{q}}(\omega) \\ \underline{\mathbf{u}}_\Sigma(\omega) \\ \underline{\mathbf{v}}_i(\omega) \end{bmatrix} = \begin{bmatrix} \underline{\boldsymbol{\mathcal{F}}}(\omega) \\ \underline{\mathbb{f}}_\Sigma(\omega) \\ \underline{\mathbf{g}}_i(\omega) \end{bmatrix} \quad , \tag{5}$$

where $\underline{\mathbf{q}}(\omega)$ is the mean vector in $\mathbb{C}^{NN_g}$ defined by $\underline{\mathbf{q}}(\omega) = \{\underline{\mathbf{q}}^0(\omega), \ldots, \underline{\mathbf{q}}^{N-1}(\omega)\}$, where $\underline{\mathbf{u}}_\Sigma(\omega)$ is the mean vector in $\mathbb{C}^{Nn_\Sigma}$ defined by $\underline{\mathbf{u}}_\Sigma(\omega) = \{\underline{\mathbf{u}}^0_\Sigma(\omega), \ldots, \underline{\mathbf{u}}^{N-1}_\Sigma(\omega)\}$ and where $\underline{\mathbf{v}}_i(\omega)$ is the mean vector of the $\mathbb{C}^{n_d - Nn_\Sigma}$ describing the internal DOFs of the disk. We have $[\underline{\mathcal{A}}(\omega)^{jk}] = [\underline{\mathcal{A}}^j(\omega)]\,\delta_{jk}$, $[\underline{A}_c(\omega)^{jk}] = [\underline{A}^j_c(\omega)]\,\delta_{jk}$ and $[\underline{A}_\Sigma(\omega)^{jk}] = [\underline{A}^j_\Sigma(\omega)]\,\delta_{jk}$, where the upper subscript jk denotes the matrix block defining the connection between blade j and blade k. The right side of Eq.(5) defines the terms related to the mean external forces.

3 Nonparametric model of random uncertainties for blade mistuning

In this Section, the nonparametric model of random uncertainties related to the blade mistuning is constructed. The main results concerning the nonparametric probability model of random uncertainties in structural dynamics [15, 16] are used. Such a probability model is implemented from the mean reduced matrix model of each blade.

3.1 Random reduced matrix model for the bladed-disk

Using the methodology derived from [15, 18], the nonparametric probabilistic approach consists in modeling the reduced dynamic stiffness matrix for blade j as the random matrix

$$[\mathbf{A}^j_{\text{red}}(\omega)] = -\omega^2[\mathbf{M}^j_{\text{red}}] + i\omega[\mathbf{D}^j_{\text{red}}] + [\mathbf{K}^j_{\text{red}}] \quad , \tag{6}$$

in which $[\mathbf{M}^j_{\text{red}}]$, $[\mathbf{D}^j_{\text{red}}]$ and $[\mathbf{K}^j_{\text{red}}]$ are $N_a \times N_a$ independent random matrices corresponding to the random reduced mass, damping and stiffness matrices of blade j. The results and notation of Section 2 are transposed for the random case. We then deduce that

$$[\mathbf{A}^j_{\text{red}}(\omega)] = \begin{bmatrix} [\boldsymbol{\mathcal{A}}^j(\omega)] & [\mathbf{A}^j_c(\omega)] \\ [\mathbf{A}^j_c(\omega)]^T & [\mathbf{A}^j_\Sigma(\omega)] \end{bmatrix} \quad , \tag{7}$$

and the random stochastic system corresponding to Eq. (5) is written as

$$\begin{bmatrix} [\boldsymbol{\mathcal{A}}(\omega)] & [\mathbf{A}_c(\omega)] & [\mathbb{0}] \\ [\mathbf{A}_c(\omega)]^T & [\mathbf{A}_\Sigma(\omega)] + [\underline{A}^d_{\Sigma\Sigma}(\omega)] & [\underline{A}^d_{i\Sigma}(\omega)]^T \\ [\mathbb{0}] & [\underline{A}^d_{i\Sigma}(\omega)] & [\underline{A}^d_{ii}(\omega)] \end{bmatrix} \begin{bmatrix} \mathbf{Q}(\omega) \\ \mathbf{U}_\Sigma(\omega) \\ \mathbf{V}_i(\omega) \end{bmatrix} = \begin{bmatrix} \underline{\boldsymbol{\mathcal{F}}}(\omega) \\ \underline{\mathbb{f}}_\Sigma(\omega) \\ \underline{\mathbf{g}}_i(\omega) \end{bmatrix} \quad , \tag{8}$$

in which $\mathbf{Q}(\omega)$, $\mathbf{U}_\Sigma(\omega)$ and $\mathbf{V}_i(\omega)$ are the $\mathbb{C}^{NN_g}$-valued random vector of the generalized coordinates, the $\mathbb{C}^{Nn_\Sigma}$-valued random vector of the DOFs of the coupling interface and the $\mathbb{C}^{n_d - Nn_\Sigma}$ random vector of the internal DOFs of the disk respectively.

3.2 Probability model of the random matrices for one blade

Since the random uncertainties are statistically independent from blade to blade, random matrices $[\mathbf{A}^0_{\text{red}}(\omega)], \ldots, [\mathbf{A}^{N-1}_{\text{red}}(\omega)]$ are statistically independent. We can limit the construction of the probability model to one blade. Then, we have to construct the probability model of the random matrices $[\mathbf{M}^j_{\text{red}}]$, $[\mathbf{D}^j_{\text{red}}]$ and $[\mathbf{K}^j_{\text{red}}]$. Since each random matrix involves both generalized coordinates and physical DOFs which are of different nature, it is necessary to construct the probability model on a matrix related to normalized quantities. A normalization of the random reduced matrix has to be done before constructing the probability model. In addition, the probability model has to be consistent with a mechanical problem and has to satisfy the following constraints which constitute the only available information: C1 the mean reduced matrix is equal to the mean value of the random reduced matrix; C2 the signature of the random reduced matrix is respected: it means that the random reduced matrix has to be positive definite (or semi-positive definite) if its corresponding mean reduced matrix is positive definite (or semi-positive definite) ; C3 the second-order moment of the physical random response of the bladed-disk has to exist. The probability model is then derived from these three constraints by using the entropy maximization principle. It should be outlined that constraints C2 and C3 do not allow the probability distribution to be independently constructed for each entry of the random matrices under consideration. Only a global approach can be used to construct the probability distribution of such random matrices. In particular constraint C2 need to construct the probability density distribution on the set of all the symmetric positive-definite matrices.

3.2.1 Normalization of random matrices $[\mathbf{M}^j_{red}]$, $[\mathbf{D}^j_{red}]$ and $[\mathbf{K}^j_{red}]$.

Constraint C1 yields

$$\mathcal{E}\left\{[\mathbf{M}^j_{\text{red}}]\right\} = [\underline{M}^j_{\text{red}}] \quad , \quad \mathcal{E}\left\{[\mathbf{D}^j_{\text{red}}]\right\} = [\underline{D}^j_{\text{red}}] \quad , \quad \mathcal{E}\left\{[\mathbf{K}^j_{\text{red}}]\right\} = [\underline{K}^j_{\text{red}}] \quad , \tag{9}$$

The normalization of random matrices $[\mathbf{M}^j_{\text{red}}]$, $[\mathbf{D}^j_{\text{red}}]$ and $[\mathbf{K}^j_{\text{red}}]$ is constructed for that the mean value of each normalized random matrix is the unity matrix. Such a construction requires the factorization of the mean matrices. Since the blade with free coupling interface is considered, mean reduced mass matrix $[\underline{M}^j_{\text{red}}]$ belongs to $\mathbb{M}^+_{N_a}(\mathbb{R})$ while mean reduced stiffness and mean damping matrices $[\underline{K}^j_{\text{red}}]$ and $[\underline{D}^j_{\text{red}}]$ belong to $\mathbb{M}^{+0}_{N_a}(\mathbb{R})$ due to rigid-body modes. The rank of matrices $[\underline{K}^j_{\text{red}}]$ and $[\underline{D}^j_{\text{red}}]$ is noted N^+_a. The Cholesky factorization of matrix $[\underline{M}^j_{\text{red}}]$ is

$$[\underline{M}^j_{\text{red}}] = [\underline{L}^j_M]^T\,[\underline{L}^j_M] \quad , \tag{10}$$

in which $[\underline{L}_M^j]$ is a real $N_a \times N_a$ upper triangular matrix. Since matrix $[\underline{K}_{\text{red}}^j]$ is semi-positive definite and diagonal, we have

$$[\underline{K}_{\text{red}}^j] = [\underline{L}_K^j]^T [\underline{L}_K^j] \quad , \tag{11}$$

in which $[\underline{L}_K]$ is a $N_a^+ \times N_a$ real diagonal matrix. Since matrix $[\underline{D}_{\text{red}}^j]$ is semi-positive definite, we have

$$[\underline{D}_{\text{red}}^j] = [\underline{L}_D^j]^T [\underline{L}_D^j] \quad , \tag{12}$$

in which $[\underline{L}_D]$ is a $N_a^+ \times N_a$ real matrix obtained by solving the spectral problem related to matrix $[\underline{D}_{\text{red}}^j]$. Each random matrix is then written as

$$[\mathbf{M}_{\text{red}}^j] = [\underline{L}_M^j]^T [\mathbf{G}_M^j] [\underline{L}_M^j] \quad , \quad [\mathbf{D}_{\text{red}}^j] = [\underline{L}_D^j]^T [\mathbf{G}_D^j] [\underline{L}_D^j] \quad , \quad [\mathbf{K}_{\text{red}}^j] = [\underline{L}_K^j]^T [\mathbf{G}_K^j] [\underline{L}_K^j] \quad , \tag{13}$$

in which $[\mathbf{G}_M^j]$, $[\mathbf{G}_D^j]$ and $[\mathbf{G}_K^j]$ are normalized random matrices such that

$$\mathcal{E}\left\{[\mathbf{G}_M^j]\right\} = [\underline{G}_M^j] = [I_{N_a}] \quad , \quad \mathcal{E}\left\{[\mathbf{G}_D^j]\right\} = [\underline{G}_D^j] = [I_{N_a^+}] \quad , \quad \mathcal{E}\left\{[\mathbf{G}_K^j]\right\} = [\underline{G}_K^j] = [I_{N_a^+}] \quad . \tag{14}$$

3.2.2 Construction of the probability model of normalized random matrices $[\mathbf{G}_M^j], [\mathbf{G}_D^j], [\mathbf{G}_K^j]$

Constraints C2 and C3 which constitute the second part of the available information is written as

$$[\mathbf{M}_{\text{red}}^j] \in \mathbb{M}_{N_a}^+(\mathbb{R}) \quad , \quad [\mathbf{D}_{\text{red}}^j] \in \mathbb{M}_{N_a}^{+0}(\mathbb{R}) \quad , \quad [\mathbf{K}_{\text{red}}^j] \in \mathbb{M}_{N_a}^{+0}(\mathbb{R}) \quad , \tag{15}$$

$$\left\{ \begin{bmatrix} \mathbf{Q}(\omega) & \mathbf{U}_\Sigma(\omega) & \mathbf{V}_i(\omega) \end{bmatrix}^T , \omega \in \mathbb{B} \right\} \text{ is a second-order stochastic process.} \tag{16}$$

It can be shown [16] that the normalized random reduced matrices have to be such that Eq. (14) holds and such that

$$[\mathbf{G}_M^j] \in \mathbb{M}_{N_a}^+(\mathbb{R}) \quad , \quad [\mathbf{G}_D^j] \in \mathbb{M}_{N_a^+}^+(\mathbb{R}) \quad , \quad [\mathbf{G}_K^j] \in \mathbb{M}_{N_a^+}^+(\mathbb{R}) \quad , \tag{17}$$

$$\mathcal{E}\left\{ ||[\mathbf{G}_M^j]^{-1}||_F^2 \right\} < +\infty \quad , \quad \mathcal{E}\left\{ ||[\mathbf{G}_D^j]^{-1}||_F^2 \right\} < +\infty \quad , \quad \mathcal{E}\left\{ ||[\mathbf{G}_K^j]^{-1}||_F^2 \right\} < +\infty \quad . \tag{18}$$

The dispersion level of these three normalized random matrices can be controlled by the positive real parameters δ_M^j, δ_D^j, δ_K^j defined by

$$\delta_E^j = \left\{ \frac{\mathcal{E}\left\{ ||[\mathbf{G}_E^j] - [\underline{G}_E^j]||_F^2 \right\}}{||[\underline{G}_E^j]||_F^2} \right\}^{\frac{1}{2}} \quad \text{with} \quad E = \{M, D, K\} \quad . \tag{19}$$

From Eq.(13), it can be deduced that these parameters allow the dispersion level of random matrices $[\mathbf{M}_{\text{red}}^j]$, $[\mathbf{D}_{\text{red}}^j]$ and $[\mathbf{K}_{\text{red}}^j]$ to be controlled. Below, $[\mathbf{G}]$ denotes $[\mathbf{G}_M^j]$, $[\mathbf{G}_D^j]$ and $[\mathbf{G}_K^j]$, n denotes N_a, N_a^+ and N_a^+ and δ denotes δ_M^j, δ_D^j and δ_K^j. Using the entropy maximization principle with available information defined by Eqs. $(14), (17)$ and (18), it can be proved [15, 16] that the probability density function of random matrix $[\mathbf{G}]$ with respect to the volume element

$$\tilde{d}G = 2^{n(n-1)/4} \prod_{1 \leqslant i \leqslant j \leqslant n} d\,[G]_{ij} \quad , \tag{20}$$

is written as

$$p_{[\mathbf{G}]}([G]) = \mathbb{1}_{\mathbb{M}_n^+(\mathbb{R})}([G]) \times C_G \times (\det([G]))^{(1-\delta^2)(2\delta)^{-1}(n+1)} \times e^{-(n+1)(2\delta)^{-1}\text{tr}([G])} \quad , \tag{21}$$

where C_G is the positive constant such that

$$C_G = \frac{(2\pi)^{-n(n-1)/4} \left(\frac{n+1}{2\delta^2}\right)^{n(n+1)(2\delta^2)^{-1}}}{\prod_{j=1}^n \Gamma(\frac{n+1}{2\delta^2} + \frac{1-j}{2})} \quad , \tag{22}$$

in which $\Gamma(z)$ is the gamma function defined for all $z > 0$ by $\Gamma(z) = \int_0^\infty t^{z-1}e^{-t}dt$. Equation (21) shows that the entries $[\mathbf{G}]_{jk}$ of random matrix $[\mathbf{G}]$ are dependent random variables. The covariance tensor $C^G_{jk,j'k'} = \mathcal{E}\{([\mathbf{G}]_{jk} - [\underline{G}]_{jk})([\mathbf{G}]_{j'k'} - [\underline{G}]_{j'k'})\}$ is such that

$$C^G_{jk,j'k'} = \frac{\delta^2}{n+1}\{\delta_{j'k}\delta_{jk'} + \delta_{jj'}\delta_{kk'}\} \quad . \tag{23}$$

The variance of random variable $[\mathbf{G}]_{jk}$ is then given by

$$V^G_{jk} = \frac{\delta^2}{n+1}(1 + \delta_{jk}) \quad . \tag{24}$$

With the available information defined by Eqs. $(14), (17)$ and (18), and using the entropy maximization principle, it can be proved that random matrices $\big\{[\mathbf{G}^j_M], [\mathbf{G}^j_D], [\mathbf{G}^j_K], j \in \{0, \ldots, N-1\}\big\}$ are independent.

3.2.3 Algebraic representation of normalized matrices $[\mathbf{G}^j_M]$, $[\mathbf{G}^j_D]$, $[\mathbf{G}^j_K]$

The following algebraic representation of random positive-definite symmetric real matrix $[\mathbf{G}]$ allows a procedure for the Monte Carlo numerical simulation of random matrix $[\mathbf{G}]$ to be defined. Random matrix $[\mathbf{G}]$ is written as

$$[\mathbf{G}] = [\mathbf{L}_G]^T[\mathbf{L}_G] \quad , \tag{25}$$

in which $[\mathbf{L}_G]$ is an $n \times n$ real upper triangular random matrix such that

(1) random variables $\{[\mathbf{L}_G]_{jj'}, j \leqslant j'\}$ are independent;

(2) for $j < j'$, real-valued random variable $[\mathbf{L}_G]_{jj'}$ can be written as $[\mathbf{L}_G]_{jj'} = \sigma_n U_{jj'}$ in which $\sigma_n = \delta(n+1)^{-1/2}$ and where $U_{jj'}$ is a real-valued Gaussian random variable with zero mean and variance equal to 1;

(3) for $j = j'$, positive-valued random variable $[\mathbf{L}_G]_{jj}$ can be written as $[\mathbf{L}_G]_{jj} = \sigma_n\sqrt{2V_j}$ in which σ_n is defined above and where V_j is a positive-valued gamma random variable whose probability density function $p_{V_j}(v)$ with respect to dv is written as

$$p_{V_j}(v) = \mathbb{1}_{\mathbb{R}^+}(v)\frac{1}{\Gamma(\frac{n+1}{2\delta^2} + \frac{1-j}{2})}v^{\frac{n+1}{2\delta^2} - \frac{1+j}{2}}e^{-v} \quad . \tag{26}$$

4 Mistuning analysis

The first reduction described in Section 2 is only justified by the use of the nonparametric approach and keeps all the physical DOFs of the disk. A second global reduction is thus necessary in order to accelerate the numerical computations.

4.1 Second modal reduction

We introduce a vector $\mathbb{Q}(\omega)$ such that

$$\begin{bmatrix} \mathbf{Q}(\omega) \\ \mathbf{U}_\Sigma(\omega) \\ \mathbf{V}_i(\omega) \end{bmatrix} = [\underline{\Psi}]\,\mathbb{Q}(\omega) \quad , \tag{27}$$

where the columns of the matrix $[\underline{\Psi}]$ are the $\tilde{n}$ eigenvectors related to the $\tilde{n}$ first eigenvalues of the mean generalized eigenvalue problem related to Eq.(5). It should be noted that these calculations are carried out by using the cyclic symmetry properties. Premultiplying Eq.(8) by $[\underline{\Psi}]^T$ and using Eq.(27) yields matrix equation

$$[\mathbb{A}(\omega)]\,\mathbb{Q}(\omega) = \underline{\mathbb{F}}(\omega) \quad . \tag{28}$$

The random vector of the physical DOFs for blade j is then given by

$$\begin{bmatrix} \mathbf{U}^j_i(\omega) \\ \mathbf{U}^j_\Sigma(\omega) \end{bmatrix} = [\underline{H}^j] \begin{bmatrix} \mathbf{Q}^j(\omega) \\ \mathbf{U}^j_\Sigma(\omega) \end{bmatrix} \quad , \tag{29}$$

in which, for blade j, $\mathbf{U}_i^j(\omega)$ is the $\mathbb{C}^{n_i}$-valued random vector of the internal DOFs, $\mathbf{U}_\Sigma^j(\omega)$ is the $\mathbb{C}^{n_\Sigma}$-valued random vector of the coupling interface DOFs and $\mathbf{Q}^j(\omega)$ is the $\mathbb{C}^{N_a}$-valued random vector of the generalized coordinates. The stochastic equation related to Eq. (28) is solved frequency-by-frequency using the Monte Carlo numerical simulation. The two bases are related to deterministic quantities concerning the mean model. It should be noted that these bases are consistent from a mathematical point of view for the stochastic system. Concerning the dimension of numerical applications, a stochastic convergence analysis with respect to the model reduction has to be performed in order to validate the numerical results.

4.2 Random magnification factor

The observation is the random dynamic magnification factor $\{\mathbf{B}(\omega), \omega \in \mathbb{B}\}$ which is the positive real-valued stochastic process indexed by $\mathbb{B}$ such that

$$\mathbf{B}(\omega) = \sup_{j\in\{0,\ldots,N-1\}} \mathbf{B}^j(\omega) \quad , \quad \mathbf{B}^j(\omega) = \frac{||\mathbf{U}^j(\omega)||}{||\underline{\mathbf{u}}^j||_\infty} \quad , \quad ||\underline{\mathbf{u}}^j||_\infty = \sup_{\omega\in\mathbb{B}} ||\underline{\mathbf{u}}^j(\omega)|| \quad , \tag{30}$$

in which, for blade j, $\mathbf{U}^j(\omega)$ is the random vector of the physical DOFs and $\underline{\mathbf{u}}^j(\omega)$ is the mean vector of the physical DOFs. The random dynamic magnification factor over narrow-frequency band $\mathbb{B}$ is defined by

$$B_\infty = \sup_{\omega\in\mathbb{B}} \mathbf{B}(\omega) \quad . \tag{31}$$

The realizations of random observation B_∞ are deduced from the Monte Carlo numerical simulations and mathematical statistics are used for estimating probability quantities related to random variable B_∞.

5 Numerical example for a bladed-disk

A simple example is presented in order to illustrate the application of the proposed nonparametric probability model of random uncertainties.

5.1 Definition of the mean finite element model

The bladed-disk considered (see Fig. 1) is constituted of a disk and 24 blades which are modeled by using linear thin plane theory in bending mode. The membrane and the bending motions are fully decoupled. We are only interested in the outplane displacements. The bladed-disk is located in the plane (Ox, Oy) of a cartesian coordinate system. It should be noted that, in the case of such a rotating structure, the outplane vibration response would not be affected by gyroscopic terms. The disk is made of a homogeneous and isotropic material with constant thickness 5×10^{-3} m, inner radius 3.5×10^{-2} m, outer radius 0.1 m, mass density 7860 kg/m^3, Poisson ratio 0.25 and Young modulus 1.89×10^{11} N/m^2. A Dirichlet condition is applied along the internal boundary defined by the inner radius. Each blade is made of a homogeneous and isotropic material with length 7×10^{-2} m, width 8.5×10^{-3} m, linear decreasing thickness from 5×10^{-3} m to 1×10^{-3} m, mass density 7860 kg/m^3, Poisson ratio 0.25 and Young modulus 2×10^{11} N/m^2. A damping model is added for the bladed-disk, corresponding to a hysteretic model with a mean loss factor $\eta = 0.0004$. The mean finite element model shown in Fig. 1 is constituted of 312 (with 4 nodes) bending plate elements and has 1296 DOFs such that the DOF number of one blade is $n_a = 36$, the DOF number of the disk is $n_d = 576$ and the DOF number of a blade-disk coupling interface is $n_\Sigma = 6$. Figure 2 displays the eigenfrequencies of the generalized eigenproblem associated with the tuned mechanical system in function of the circumferential wave number m. A frequency "veering" can clearly be seen and leads us to choose the frequency band of analysis $\mathbb{B} = [7040, 7200]$ Hz corresponding to a circumferential wave number $m = 4$. A 4 engine order excitation is then applied to excite the modes of the veering zone. Each blade j is submitted to a unit transverse load vector $\underline{\mathbf{f}}^j(\omega)$ such that

$\underline{\mathbf{f}}^j(\omega)_k = \mathbb{1}_{\mathbb{B}}(\omega)\delta_{k,(2d+1)}e^{(2i\pi m j)/N}$ in which $m = 4$ and where d is the node number of the applied force. Concerning the nonparametric probability model, it is assumed that $\delta_M^j = \delta_D^j = 0$ for all the blades (no uncertainty in mass and damping) The mistuning is introduced by fixing the value $\delta_K^j = \delta_K$ for the blades (uncertainty in stiffness). For the parametric approach, standard deviation $\sigma_K^j = \sigma$ is deduced from Eq. (41). Let $\nu = \omega/(2\pi)$ be the circular frequency associated with angular frequency ω. As an example, for the nonparametric model with $\delta_K = 0.01$, Fig. 3 shows the graph of the tuned response (dashed thick line), the graph of one realization of the random responses of the 24 blades (thin lines) and of its upper bound (thick line) with respect to frequency band $\mathbb{B}$. Figure 4 shows a realization of $B^j(\omega)$ for the frequency $\nu = 7108.9$ Hz which corresponds to the largest amplification that can occur in band $\mathbb{B}$. The well known localization phenomenon is exhibited for blades 11 and 12 for which the largest amplifications is obtained.

5.2 Convergence analysis

A convergence analysis has been carried out. Since the second-order mean convergence yields the convergence in law, the convergence analysis can be limited to the second-order convergence of the sequence $\{\mathbf{B}(\omega_0, N_g, \tilde{n})\}_{N_g,\tilde{n}}$ of random variables, that is to say to construct the function $(N_g, \tilde{n}) \mapsto |||\mathbf{B}(\omega_0, N_g, \tilde{n})|||$ in which $\omega_0 = 2\,\pi\,\nu_0$ is a fixed frequency and where

$$|||\mathbf{B}(\omega_0, N_g, \tilde{n})|||^2 = \mathcal{E}\{\mathbf{B}(\omega_0, N_g, \tilde{n})^2\}. \tag{32}$$

This norm is estimated by $|||\mathbf{B}(\omega_0, N_g, \tilde{n})||| \simeq \text{Conv}(n_s, N_g, \tilde{n})$ in which

$$\text{Conv}(n_s, N_g, \tilde{n})^2 = \frac{1}{n_s}\sum_{i=1}^{n_s} \mathbf{B}(\omega_0, N_g, \tilde{n}, \theta_i)^2 \quad , \tag{33}$$

where θ_i is realization number i and where n_s is the number of realizations used in the Monte Carlo numerical simulation. Figure 5 shows the graph $n_s \mapsto \text{Conv}(n_s, N_g, \tilde{n})$ for several values of the couple $(N_g, \tilde{n})$ and for $\nu_0 = 7108$ Hz. A good convergence is obtained for $n_s = 1500$,$N_g = 8$ and $\tilde{n} = 120$. These numerical parameters are used for all the computations.

5.3 Comparison with the usual probability parametric approach

In order to give an information on the differences between the nonparametric probabilistic approach and a parametric probabilistic one, a numerical comparison is carried out. We choose as the usual parametric probability model, the Young modulus uncertainties of the blades which yield the blade eigenfrequencies mistuning. Such an approach leads the random stiffness matrix to be written as

$$[\mathbf{K}^j] = (1 + \Lambda_K^j)\,[\underline{K}^j] \quad , \tag{34}$$

where $1 + \Lambda_K^j$, which is proportional to the Young modulus, is a real-valued random variable whose probability distribution is uniform with a mean value equal to 1. Its standard deviation σ_K^j is such that $1 + \Lambda_K^j$ remains positive almost surely. The random reduced stiffness matrix $[\mathbf{K}_{\text{red}}^{j,\text{para}}]$ related to the parametric probability model of blade j is given by

$$[\mathbf{K}_{\text{red}}^{j,\text{para}}] = [\underline{L}_K^j]^T\,[\mathbf{G}_K^{j,\text{para}}]\,[\underline{L}_K^j] \quad , \quad [\mathbf{G}_K^{j,\text{para}}] = (1 + \Lambda_K^j)\,[I_{N_a^+}] \quad . \tag{35}$$

From Eqs. (34) and (35), we deduce that

$$\mathcal{E}\{[\mathbf{K}_{\text{red}}^{j,\text{para}}]\} = [\underline{K}_{\text{red}}^j] \quad . \tag{36}$$

Parameter $W_K^{j,\text{para}}$ is then introduced such that

$$\begin{aligned} W_K^{j,\text{para}} &= \mathcal{E}\{|||[\mathbf{K}_{\text{red}}^{j,\text{para}}] - [\underline{K}_{\text{red}}^j]|||_F^2\} \quad , \\ &= \mathcal{E}\{|||[\underline{L}_K^j]^T\,\left([\mathbf{G}_K^{j,\text{para}}] - [I]\right)\,[\underline{L}_K^j]|||_F^2\} \quad . \end{aligned} \tag{37}$$

This scalar parameter measures the dispersion of random reduced stiffness matrix $[\mathbf{K}_{\text{red}}^{j,\text{para}}]$. It can easily be seen that $W_K^{j,\text{para}}$ is equal to the sum of the second-order moments of the eigenvalues of the matrix $[\underline{L}_K^j]^T \left([\mathbf{G}_K^{j,\text{para}}] - [I]\right) [\underline{L}_K^j]$. Since Λ_K^j is a centered random variable and since $|||[\underline{K}_{\text{red}}^j]|||_F^2 = \text{tr}([\underline{K}_{\text{red}}^j]^2)$, Eq. (37) yields

$$W_K^{j,\text{para}} = (\sigma_K^j)^2 \, \text{tr}([\underline{K}_{\text{red}}^j]^2) \quad . \tag{38}$$

In order to establish the comparison between the two probability approaches, the similar parameter W_K^j defined by $W_K^j = \mathcal{E}\{|||[\underline{L}_K^j]^T \left([\mathbf{G}_K^j] - [I]\right) [\underline{L}_K^j]|||_F^2\}$ is introduced. Using Eqs. (13), (23) and (24) yields

$$W_K^j = \frac{(\delta_K^j)^2}{N_a^+ + 1} (\text{tr}([\underline{K}_{\text{red}}^j])^2 + \text{tr}([\underline{K}_{\text{red}}^j]^2)) \quad , \tag{39}$$

in which δ_K^j is the parameter controlling the dispersion of random matrix $[\mathbf{G}_K^j]$. From Eqs. (9) and (36), we deduce that both random stiffness matrices $[\mathbf{K}_{\text{red}}^j]$ and $[\mathbf{K}_{\text{red}}^{j,\text{para}}]$ have the same mean value,

$$\mathcal{E}\{[\mathbf{K}_{\text{red}}^j]\} = \mathcal{E}\{[\mathbf{K}_{\text{red}}^{j,\text{para}}]\} = [\underline{K}_{\text{red}}^j] \quad . \tag{40}$$

For given σ_K^j, the equation allowing the calculation of δ_K^j is obtained in writing that $W_K^j = W_K^{j,\text{para}}$ and yields

$$(\sigma_K^j)^2 = \frac{(\delta_K^j)^2}{N_a^+ + 1} \left(1 + \frac{\text{tr}([\underline{K}_{\text{red}}^j])^2}{\text{tr}([\underline{K}_{\text{red}}^j]^2)}\right) \quad . \tag{41}$$

5.4 Probability density function at a given frequency

The objective of this paper being to introduce a new nonparametric probabilistic approach of random uncertainties for blade mistuning analysis, the presentation is limited to a simple case (it is clear that this method is particularly well adapted to complex situations). In this condition, the probabilistic approaches are limited to homogeneous stiffness uncertainties from one blade to another one such that $\delta_K^j = \delta_K$ and $\sigma_K^j = \sigma_K$, for all j in $\{0, \ldots, N-1\}$. The sensitivity of $\mathbf{B}(\omega_0)$ at frequency $\nu_0 = 7108$ Hz is analyzed with respect to parameter δ_K. Equation (41) allows δ_K to be calculated giving standard deviation σ_K, such that $\delta_K = 0.01$ for σ_K fixed and equal to 0.055. The mistuning analysis is then carried out for the random magnification factor $\mathbf{B}^{\text{para}}(\omega_0^{\text{para}})$ at frequency $\nu_0^{\text{para}} = 7108.2$ Hz defined hereinafter. Frequencies ν_0 and ν_0^{para} are the frequencies for which the extreme values statistics over frequency band $\mathbb{B}$ are maximum and have been calculated using the Monte Carlo numerical simulation with 4000 realizations. We are then interested in comparing the density probability functions $p_{B(\omega_0)}(b, \omega_0)$ and $p_{B^{\text{para}}(\omega_0^{\text{para}})}(b, \omega_0^{\text{para}})$. Figure 6 shows the probability density functions $p_{B(\omega_0)}(b, \omega_0)$ and $p_{B^{\text{para}}(\omega_0^{\text{para}})}(b, \omega_0^{\text{para}})$ with $n_s = 8\,500\,000$ realizations in order to observe the largest amplifications that can occur. The support of the probability density function of the random magnification factor seems to be upper bounded by a finite value which is close to 3. This value can be compared to the value $(1 + \sqrt{N})/2 \simeq 2.95$ proposed by Whitehead [3]. But for other values of δ_K, there are frequencies for which the upper bound is greater than 2.95. It is observed that the probability density function of random magnification factor $\mathbf{B}(\omega_0)$ for the nonparametric probability model differs from the probability density function of random magnification factor $\mathbf{B}^{\text{para}}(\omega_0)$ for the parametric one.

5.5 Probability density function over frequency band $\mathbb{B}$

A mistuning analysis is then carried out for the real positive random variable B_∞. Figures 7 to 9 show the probability density functions $b \mapsto p_{B_\infty}(b)$ and $b \mapsto p_{B_\infty^{\text{para}}}(b)$ of random variables B_∞ and B_∞^{para} for $n_s = 1500$ realizations and for several mistuning rates of the nonparametric model: $\delta_K = 0.01$, $\delta_K = 0.02$ and $\delta_K = 0.04$, corresponding to $\sigma_K = 0.0055$, $\sigma_K = 0.011$ and $\sigma_K = 0.022$ for the parametric model. Below, $\mathcal{P}(A)$ denotes the probability of event A. Figures 10 to 12 show the corresponding mappings $b \mapsto \mathcal{P}(B_\infty > b)$ and $b \mapsto \mathcal{P}(B_\infty^{\text{para}} > b)$ in a logarithmic scale where

b is a the magnification factor level. The thick (or thin) lines are related to the nonparametric (or parametric) approach. These probability density functions are different. The maxima of probability density functions $p_{B_\infty}(b)$ and $p_{B_\infty^{\text{para}}}(b)$ do not occur for the same value of b. In particular, for this simple example, it can be seen that the probability density function for the nonparametric approach is shifted to the right and predicts larger magnification factors than the parametric approach. Furthermore, although the random uncertainties have the same dispersion level for both probability models, probability density function $p_{B_\infty}(b)$ has a larger dispersion than probability density function $p_{B_\infty^{\text{para}}}(b)$. Consequently, the extreme values of the random magnification factor are larger for the nonparametric approach. A comparative parametric study with respect to the mistuning rate is done for both probability models. We are interested in studying $\mathcal{P}(B_\infty \leqslant b_p) = p$ and $\mathcal{P}(B_\infty^{\text{para}} \leqslant b_p) = p$ where b_p denotes the maximum magnification level reached with a probability p. In Fig. 13, the thick (or thin) lines represent $\delta_K \mapsto b_p(\delta_K)$ for the nonparametric (or parametric) model. The lower, middle and upper curves are related to the probability level $p = 0.05$, $p = 0.50$ and $p = 0.95$ respectively. For both probability models, the amplification of the forced response presents a local maximum for a weak mistuning rate. Nevertheless, these local maxima are obtained for different mistuning rates according to the probability model used. Secondly, the sensitivity of the random magnification factor is analyzed with respect to the mean loss factor η. For a mistuning rate $\delta_K = 0.02$, Fig. 14 shows the graph $\eta \mapsto E\{B_\infty\}$ (thick line) and $\eta \mapsto E\{B_\infty^{\text{para}}\}$ (thin line). Figure 15 shows the graph $\eta \mapsto \sigma_{B_\infty}$ (thick line) and $\eta \mapsto \sigma_{B_\infty^{\text{para}}}$ (thin line).

6 Conclusion

In this paper, a nonparametric probability model of random uncertainties is proposed in order to analyze the mistuned bladed-disks. By construction, the nonparametric probabilistic approach allows both data uncertainties and model uncertainties to be taken into account. Since the objective of such a nonparametric approach of random uncertainties is to take into account the model errors, it is natural that a parameter without direct physical meaning such as δ parameter, appears in the probability model. In return, such a new parameter has to be identified for such a dynamic system or can be used as a global parameter to analyze the sensitivity to random data and model uncertainties. With such a nonparametric probability model of random uncertainties, the random eigenvalues and the associated random eigenvectors of each uncertain blade are statistically dependent and result from a single random model. In order to validate the proposed probability model, a simple example is presented, and this model is compared with a usual parametric probability model of random uncertainties. For a given frequency and for a given narrow frequency band, the numerical comparison carried out for this simple example exhibits some differences concerning the probability distributions of the random magnification factor.

Nomenclature

n_a	number of DOFs of a blade
n_d	number of DOFs of the disk
n_i	number of internal DOFs of a blade
n_Σ	number of coupling interface DOFs of a blade
$\tilde{n}$	dimension of the second global reduction
$\underline{\mathbf{q}}(\omega)$	mean vector of the generalized coordinates for all the blades
$\underline{\mathbf{q}}^j(\omega)$	mean vector of the generalized coordinates of blade j
$\underline{\mathbf{u}}_i^j(\omega)$	mean vector of the internal DOFs of blade j
$\underline{\mathbf{u}}_\Sigma(\omega)$	mean vector of the coupling interface DOFs for all the blades
$\underline{\mathbf{u}}_\Sigma^j(\omega)$	mean vector of the coupling interface DOFs of blade j
$\underline{\mathbf{v}}_i(\omega)$	mean vector of the internal DOFs of the disk
$[\underline{A}^d(\omega)]$	mean dynamic stiffness matrix of the disk
$[\underline{A}^j_{\text{red}}(\omega)]$	mean reduced dynamic stiffness matrix of blade j
$[\mathbf{A}^j_{\text{red}}(\omega)]$	random reduced dynamic stiffness matrix of blade j
$\mathbb{B}$	frequency band of analysis
$\mathbf{B}^j(\omega)$	random dynamic magnification factor of blade j
$\mathbf{B}(\omega)$	random dynamic magnification factor of the blades
$\mathbf{B}_\infty$	random dynamic magnification factor of the blades and over frequency band $\mathbb{B}$
$[\mathbf{G}_M^j]$, $[\mathbf{G}_D^j]$, $[\mathbf{G}_K^j]$	random normalized mass, damping and stiffness matrices
$[\mathbf{G}]$	representing $[\mathbf{G}_M^j]$, $[\mathbf{G}_D^j]$, $[\mathbf{G}_K^j]$
$[\underline{H}^j]$	transformation matrix issued from the Craig & Bampton decomposition
$[\underline{M}^j_{\text{red}}]$, $[\underline{D}^j_{\text{red}}]$, $[\underline{K}^j_{\text{red}}]$	mean reduced mass, damping and stiffness matrices of blade j
$[\mathbf{M}^j_{\text{red}}]$, $[\mathbf{D}^j_{\text{red}}]$, $[\mathbf{K}^j_{\text{red}}]$	random reduced mass, damping and stiffness matrices of blade j
N	number of blades
N_g	number of fixed coupling interface modes of the disk
N_a	rank of the reduced mass matrix of the blade
N_a^+	rank of the reduced damping and stiffness matrices of the blade
$\mathbb{Q}(\omega)$	random vector of the second global generalized coordinates
$\mathbf{Q}(\omega)$	random vector of the generalized coordinates for all the blades
$\mathbf{Q}^j(\omega)$	random vector of the generalized coordinates of blade j
$\mathbf{U}_i^j(\omega)$	random vector of the internal DOFs of blade j
$\mathbf{U}_\Sigma(\omega)$	random vector of the coupling interface DOFs for all the blades
$\mathbf{U}_\Sigma^j(\omega)$	random vector of the coupling interface DOFs of blade j
$\mathbf{V}_i(\omega)$	random vector of the internal DOFs of the disk
$\delta_M^j, \delta_D^j, \delta_K^j$	dispersion parameters related to the random mass, damping, stiffness matrices
δ	representing $\delta_M^j, \delta_D^j, \delta_K^j$
η	mean loss factor
ν_0	fixed frequency used in the probability nonparametric approach
ω_0	representing $2\,\pi\,\nu_0$
Σ_j	blade-disk coupling interface

$[\underline{\Psi}]$	transformation matrix issued from the second global reduction
Ω	bladed-disk
Ω_d	disk
Ω_j	blade j
$[A]^T$	transpose of matrix $[A]$
tr$([A])$	trace of matrix $[A]$
det$([A])$	determinant of square matrix $[A]$
$\|\|\mathbf{U}(\omega)\|\|$	Hermitian norm of vector $\mathbf{U}(\omega)$ such that $\|\|\mathbf{U}(\omega)\|\| = (\mathbf{U}(\omega)^T\mathbf{U}(\omega))^{1/2}$
$\|\|\mathbf{U}\|\|_\infty$	Infinity norm of vector $\mathbf{U}(\omega)$ such that $\|\|\mathbf{U}\|\|_\infty = \sup_\omega \|\|\mathbf{U}(\omega)\|\|$
$\|\|[A]\|\|_F$	Frobenius norm of matrix $[A]$ such that $\|\|[A]\|\|_F = \text{tr}([A][A]^T)^{1/2}$
$[I_n]$	$n \times n$ identity matrix
$\mathcal{E}$	mathematical expectation
$\mathbb{M}_n^+(\mathbb{R})$	set of all the positive-definite symmetric $n \times n$ real matrices
$\mathbb{M}_n^{+0}(\mathbb{R})$	set of all the positive (semi-positive definite) symmetric $n \times n$ real matrices
$\mathcal{P}(X < x)$	probability that $\{ X < x \}$
δ_{ij}	Kronecker symbol such that $\delta_{ij} = 1$ if $i = j$ and $\delta_{ij} = 0$ if $i \neq j$
$\mathbb{1}_B(b)$	indicatrix function on any set B such that $\mathbb{1}_B(b) = 1$ if $b \in B$ and $\mathbb{1}_B(b) = 0$ if $b \notin B$

References

[1] Thomas, D.L., 1979, “Dynamics of rotationnaly periodic structures”, International Journal for Numerical Methods in Engineering, **14**, pp. 81–102.

[2] Ohayon, R. and Soize, C., 1998, Structural acoustics and vibration, Academic press.

[3] Whitehead, D.S., 1966, “Effects of mistuning on the vibration of turbomachine blades induced by wakes”, Journal of Mechanical Engineering Science, **8**(1), pp. 15–21.

[4] Ewins, D.J., 1969, “The effects of detuning upon the forced vibrations of bladed disks”, Journal of Sound and Vibration, **9**(1), pp. 65–69.

[5] Wei, S.T. and Pierre, C., 1988, “Localization phenomena in mistuned assemblies for cyclic symmetry - part ii: forced vibrations”, ASME Journal of Vibration, Acoustics, Stress, and Reliability in Design, **110**(4), pp. 439–449.

[6] Lin, C.C. and Mignolet, M.P., 1996, “Effects of damping and damping mistuning on the forced vibration response of bladed disks”, Journal of Sound and Vibration, **193**(2), pp. 525–543.

[7] Lin, C.C. and Mignolet, M.P., 1997, “An adaptative perturbation scheme for the analysis of mistuned bladed disks”, ASME Journal of Engineering for Gas Turbines and Power, **119**(1), pp. 153–160.

[8] Griffin, J.H. and Hoosac, T.M., 1984, “Model development and statistical investigation of turbine blade mistuning”, ASME Journal of Vibration, Acoustics, Stress, and Reliability in Design, **106**, pp. 204–210.

[9] Mignolet, M.P. and Lin, C.C., 1993, “The combined closed form-perturbation approach to the analysis of mistuned bladed disks”, ASME Journal of Turbomachinery, **115**, pp. 771–780.

[10] Yang, M-T. and Griffin, J.H., 2001, “A reduced-order model of mistuning using a subset of nominal modes”, ASME Journal of Engineering for Gas Turbines and Power, **123**(3), pp. 893–900.

[11] Bladh, R., Castanier, M.P., and Pierre, C., 2001, “Component-mode-based reduced order modeling techniques for mistuned bladed disks-part 1: Theoretical models”, ASME Journal of Engineering for Gas Turbines and Power, **123**(1), pp. 89–99.

[12] Seinturier, E., Dupont, C., Berthillier, M., and Dumas, M., 2002, “A new aeroelastic model for mistuned bladed disks”, in “AIAA paper 2002-1533”, 43rd AIAA/ASME/ASCE/AHS/ASC Structures, Structural Dynamics, and Materials Conference.

[13] Mignolet, M.P., Rivas-Guerra, A.J., and Delor, J.P., 2001, “Identification of mistuning characteristics of bladed disks from free response data (part 1)”, ASME Journal of Engineering for Gas Turbines and Power, **123**, pp. 395–403.

[14] Rivas-Guerra, A.J., Mignolet, M.P., and Delor, J.P., 2001, “Identification of mistuning characteristics of bladed disks from free response data (part 2)”, ASME Journal of Engineering for Gas Turbines and Power, **123**(2), pp. 404–411.

[15] Soize, C., 2000, “A nonparametric model of random uncertainties for reduced matrix models in structural dynamics”, Probabilistic Engineering Mechanics, **15**(3), pp. 277–294.

[16] Soize, C., 2001, “Maximum entropy approach for modeling random uncertainties in transient elastodynamics.”, Journal of the Acoustical Society of America, **109**(5), pp. 1979–1996.

[17] Craig, R.R.Jr. and Bampton, M.C.C., 1968, “Coupling of substructures for dynamic analyses”, AIAA Journal, **6**(7), pp. 1313–1319.

[18] Soize, C. and Chebli, H., 2003, “Random uncertainties model in dynamic substructuring using a nonparametric probabilistic model.”, ASCE Journal of Engineering Mechanics, **129**(4), pp. 449–457.

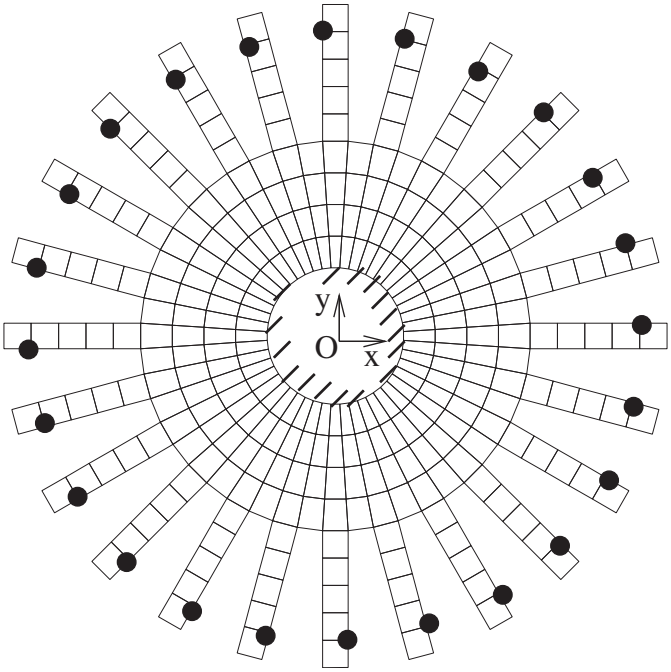

Figure 1

Fig. 1. Finite element mesh of the bladed-disk. Input force localization (symbol •)

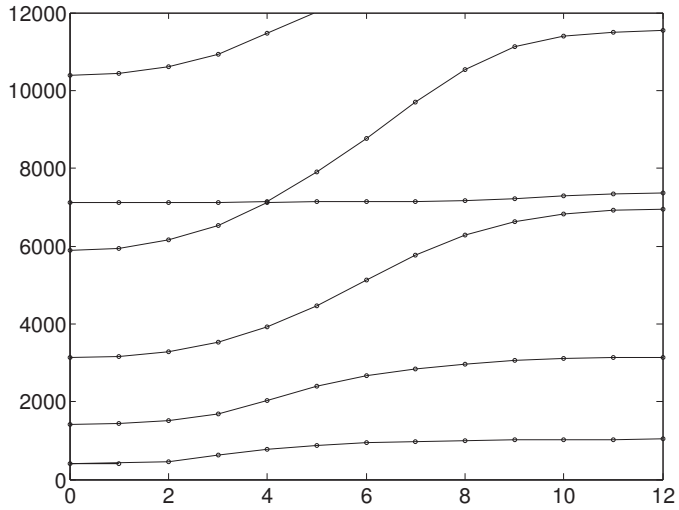

Figure 2

Fig. 2. Graph of the eigenfrequencies values (in Hz) of the tuned bladed-disk versus the circumferential wave number m.

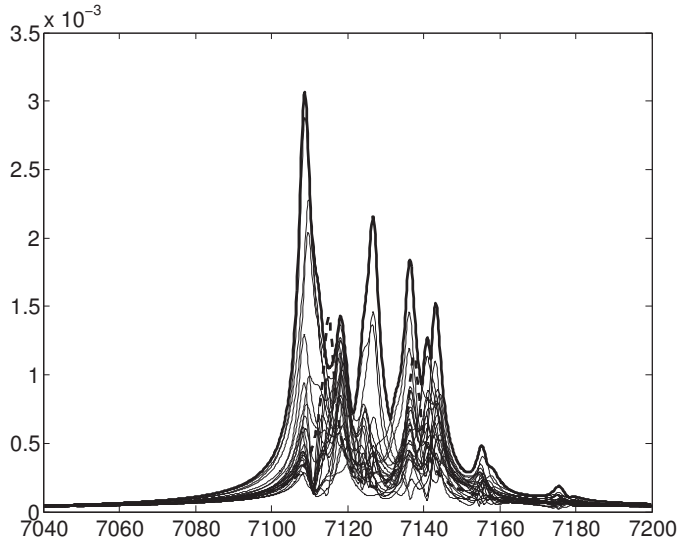

Figure 3

Fig. 3. (1) Displacement forced response (m) of the tuned system with respect to the excitation frequency (Hz): $\nu \mapsto ||\underline{\mathbf{u}}^a(\nu)||$ (thick dashed line). (2) Graph of one realization θ_1 of the random displacement forced response (m) with respect to the excitation frequency (Hz): $\nu \mapsto \max_{j\in\{0,\ldots,N-1\}} ||\mathbf{U}^j(\nu,\theta_1)||$ (thick line), $\nu \mapsto ||\mathbf{U}^j(\nu,\theta_1)||, j \in \{0,\ldots,N-1\}$ (thin lines).

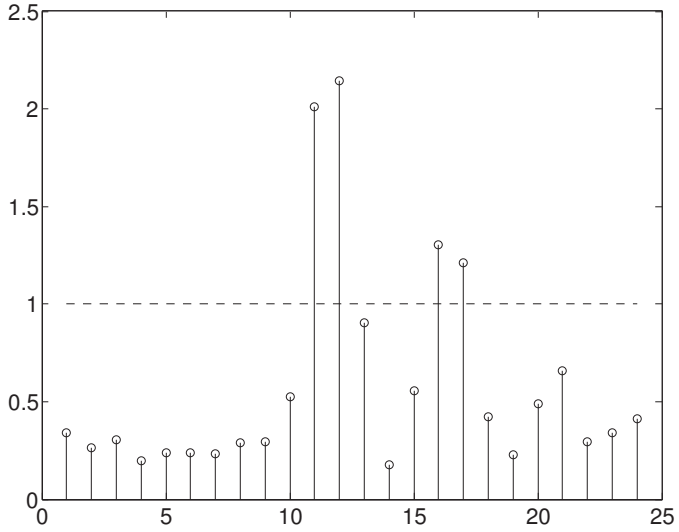

Figure 4

Fig. 4. Spatial localization: graph of one realization θ_1 of magnification factor $j \mapsto \mathbf{B}^j(\nu, \theta_1)$ for all the blades.

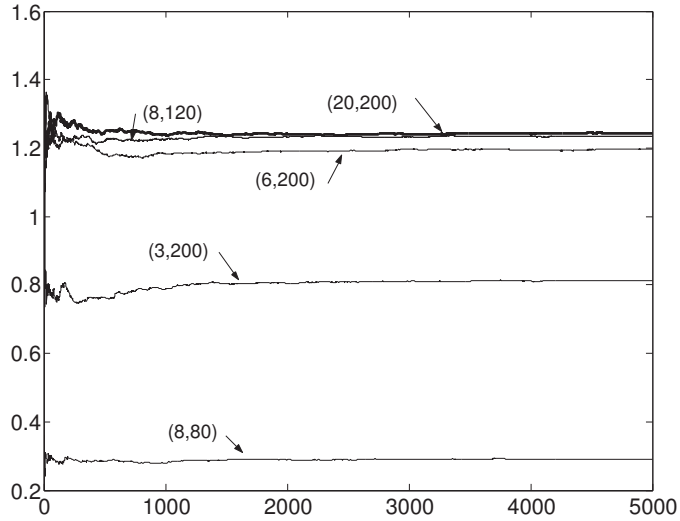

Figure 5

Fig. 5. Convergence analysis: graph of functions $n_s \mapsto \text{Conv}(n_s, N_g, \tilde{n})$ for several values of the couple $(N_g, \tilde{n})$.

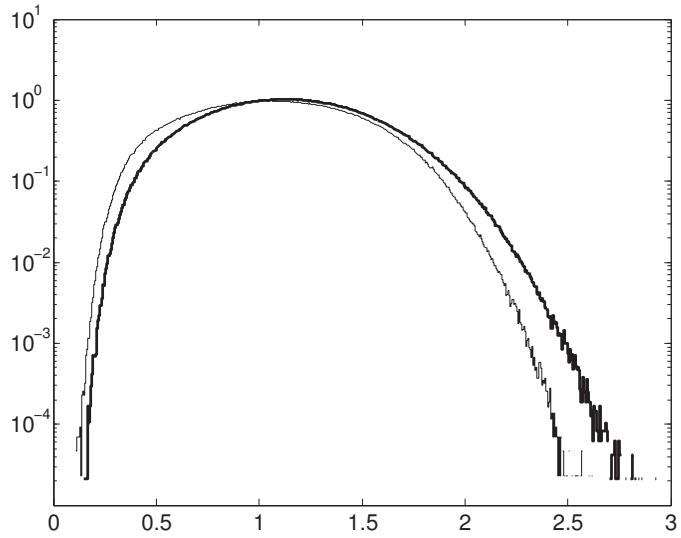

Figure 06

Fig. 06. Comparison of the nonparametric and the parametric models: probability density functions of random magnification factors $\mathbf{B}(\omega_0)$ and $\mathbf{B}^{\text{para}}(\omega_0^{\text{para}})$ in a logarithmic scale: $b \mapsto p_{B(\omega_0)}(b, \omega_0)$ (thick line), $b \mapsto p_{B^{\text{para}}(\omega_0^{\text{para}})}(b, \omega_0^{\text{para}})$ (thin line).

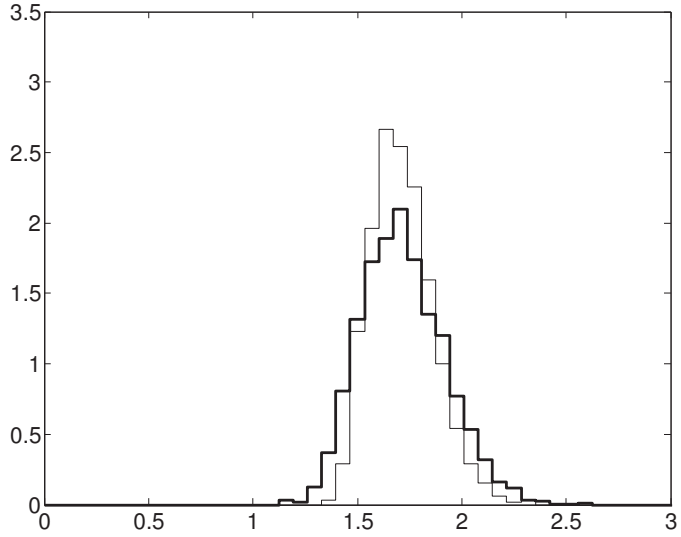

Figure 07

Fig. 07. Comparison of the nonparametric and the parametric models: graphs of the probability density functions $b \mapsto p_{B_\infty}(b)$ (thick line) and $b \mapsto p_{B_\infty^{\text{para}}}(b)$ (thin line) for $\delta_K = 0.01$.

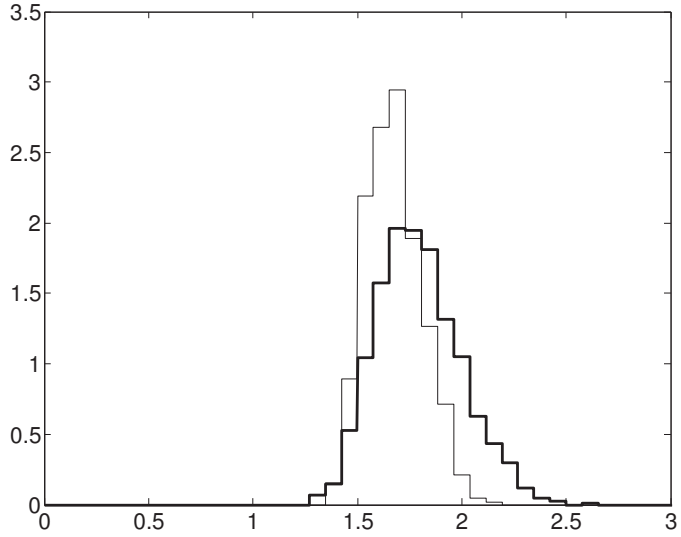

Figure 08

Fig. 08. Comparison of the nonparametric and the parametric models: graphs of the probability density functions $b \mapsto p_{B_\infty}(b)$ (thick line) and $b \mapsto p_{B_\infty^{\text{para}}}(b)$ (thin line) for $\delta_K = 0.02$.

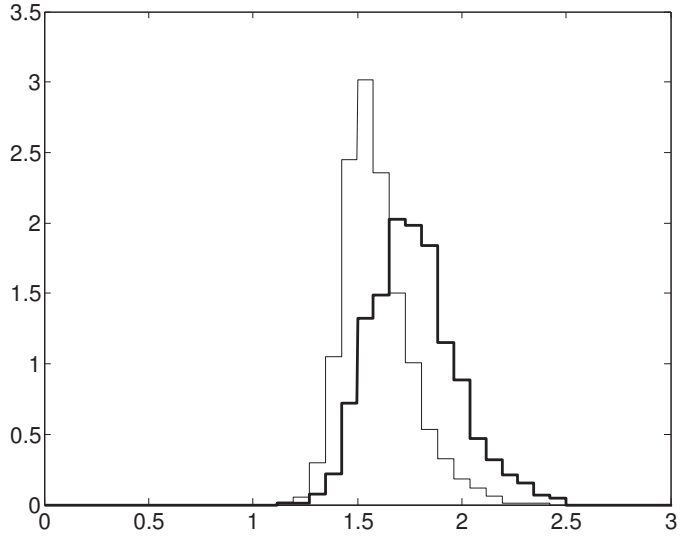

Figure 09

Fig. 09. Comparison of the nonparametric and the parametric models: graphs of the probability density functions $b \mapsto p_{B_\infty}(b)$ (thick line) and $b \mapsto p_{B_\infty^{\text{para}}}(b)$ (thin line) for $\delta_K = 0.04$.

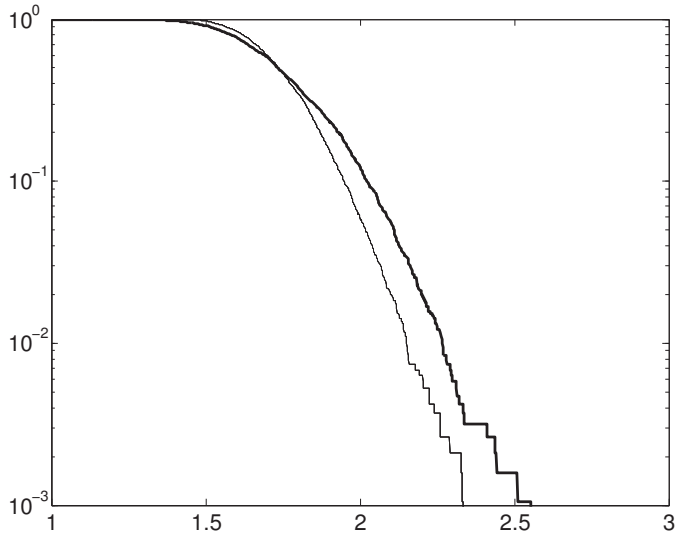

Figure 10

Fig. 10. Comparison of the nonparametric and the parametric models: graphs of $b \mapsto \mathcal{P}(B_\infty > b)$ (thick line), $b \mapsto \mathcal{P}(B_\infty^{\text{para}} > b)$ (thin line) in a logarithmic scale for $\delta_K = 0.01$.

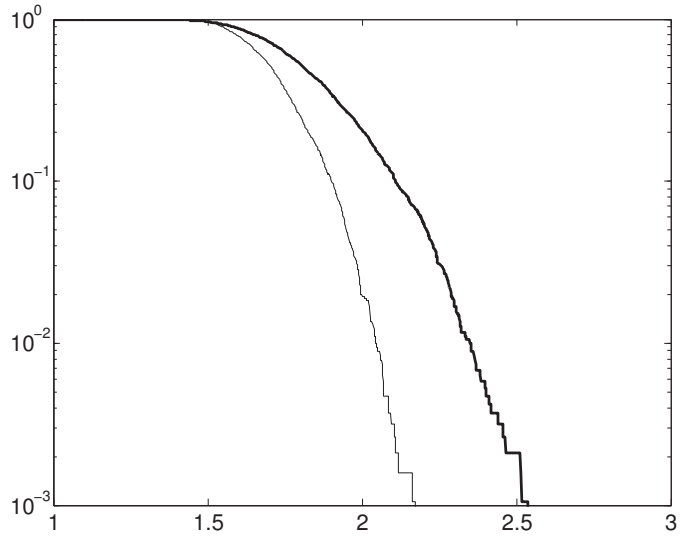

Figure 11

Fig. 11. Comparison of the nonparametric and the parametric models: graphs of $b \mapsto \mathcal{P}(B_\infty > b)$ (thick line), $b \mapsto \mathcal{P}(B_\infty^{\text{para}} > b)$ (thin line) in a logarithmic scale for $\delta_K = 0.02$.

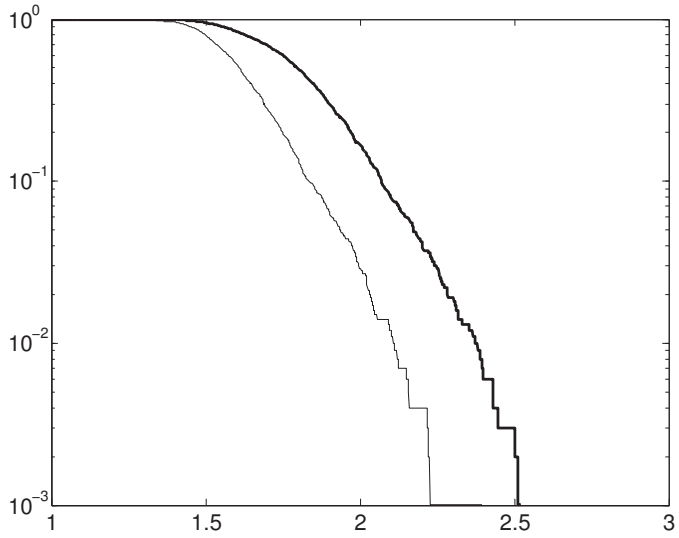

Figure 12

Fig. 12. Comparison of the nonparametric and the parametric models: graphs of $b \mapsto \mathcal{P}(B_\infty > b)$ (thick line), $b \mapsto \mathcal{P}(B_\infty^{\text{para}} > b)$ (thin line) in a logarithmic scale for $\delta_K = 0.04$.

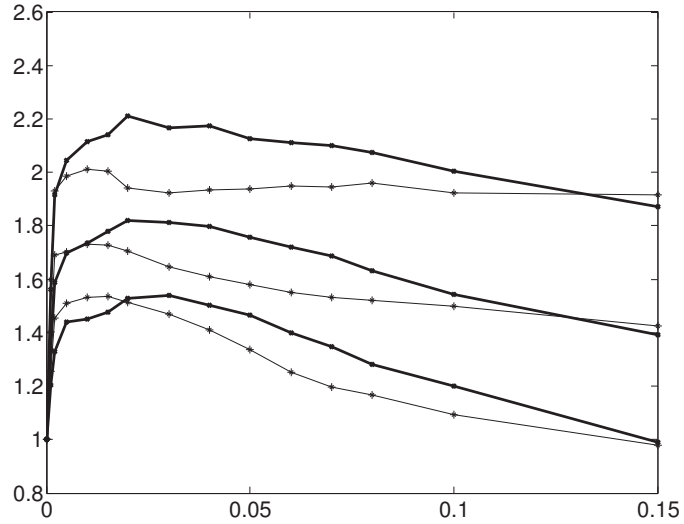

Figure 13

Fig. 13. Influence of the mistuning rate: graph of $\delta_K \mapsto b_p(\delta_K)$ such that $\mathcal{P}(B_\infty \leqslant b_p) = p$. The thick (or thin) lines are related to the nonparametric (or parametric) model (the lower, middle and upper curves correspond respectively to $p = 0.05$, $p = 0.5$ and $p = 0.95$).

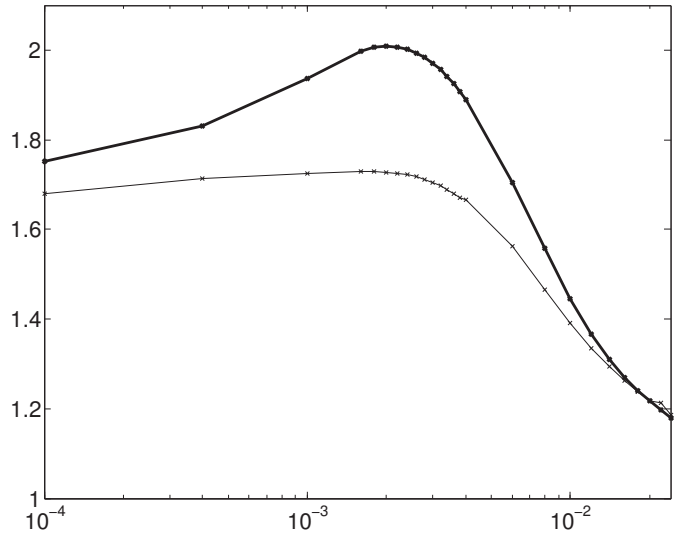

Figure 14

Fig. 14. Influence of the mean loss factor for a mistuning rate $\delta_K = 0.02$: graphs of $\eta \mapsto E\{B_\infty\}$ (thick line), $\eta \mapsto E\{B_\infty^{\text{para}}\}$ (thin line).

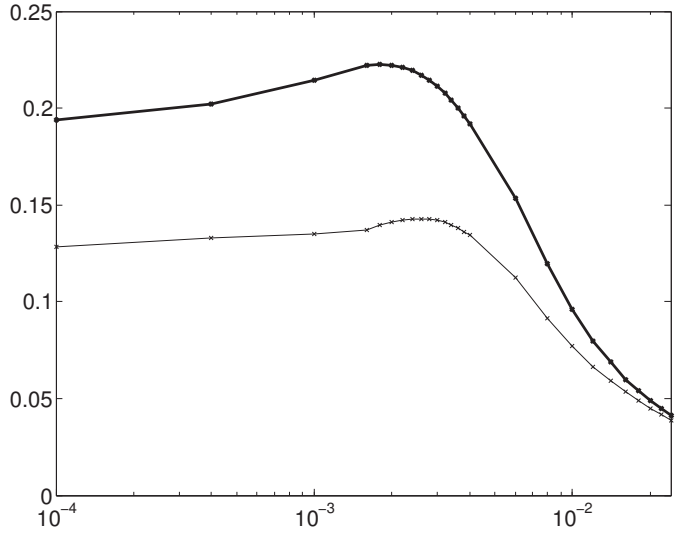

Figure 15

Fig. 15. Influence of the mean loss factor for a mistuning rate $\delta_K = 0.02$: graphs of $\eta \mapsto \sigma_{B_\infty}$ (thick line), $\eta \mapsto \sigma_{B_\infty^{\text{para}}}$ (thin line).

List of Figures